Int. J. Heat Mass Transfer. Vol. 14, pp. 1295–1309. Pergamon Press 1971. Printed in Great Britain

# COMBINED FREE AND FORCED CONVECTIVE HEAT TRANSFER AND FLUID FLOW IN A ROTATING CURVED CIRCULAR TUBE

H. MIYAZAKI

Department of Mechanical Engineering, University of Minnesota, Minneapolis, Minnesota, U.S.A.

(*Received* 11 *August* 1970 *and in revised form* 13 *November* 1970)

**Abstract**—A study is made of the combined free and forced convective heat transfer and fluid flow in a rotating curved circular tube for the fully developed flow with the thermal boundary condition of constant heat flux per unit length of tube. The heat-transfer and flow-friction characteristics are determined by the five non-dimensional parameters, i.e. the radius ratio $B$, the Prandtl number $Pr$, a parameter $Ro$ which represents the effects of Coriolis forces, the Grashof number $Gr_2$ and the Dean number $K_1$. The governing equations are solved by finite difference method, and the results of computations are presented for the axial velocity and temperature distributions, the streamlines and isothermals, the local $f$ and $Nu$, and the mean $f$ and $Nu$. The effects of $B$ is minor. $Pr$ has substantially no effect on $f$, but increases $Nu$ greatly when a strong secondary current is present. The increase in the last three parameters of secondary-flow-inducing forces enhance both $f$ and $Nu$ significantly. The rate of increase in $f$ and $Nu$ due to the force parameters is higher for a circular tube than for rectangular tubes. Their effects commence to be pronounced at smaller values of them which are $Ro \approx 2$, $Gr_2 \approx 100$ and $K_1 \approx 100$, while those for a square tube are $Ro \approx 10$, $Gr_2 \approx 1000$ and $K_1 \approx 100$.

## NOMENCLATURE

$a$, radius of circular tube;
$b$, radius of curvature;
$B$, radius ratio $\equiv b/a$;
$c_p$, specific heat at constant pressure;
$C$, source term;
$C_1$, pressure gradient in $\varphi$-direction;
$C_2$, temperature gradient in $\varphi$-direction;
$D, E, F$, dummy functions;
$f$, friction factor;
$f_c$, centrifugal acceleration $= b\Omega^2$;
$Gr_2$, Grashof number $\equiv \beta f_c \Delta t_2 a^3/\nu^2$;
$h$, heat-transfer coefficient;
$k$, thermal conductivity;
$K_1$, Dean number $\equiv 2aw_1/(\nu\sqrt{B})$;
$M, N$, number of divisions in $R$- and $\theta$-directions;
$Nu$, Nusselt number $\equiv 2ah/k$;
$p$, pressure;
$p'$, modified pressure;
$P$, non-dimensional pressure $\equiv p'/\rho\,(\nu/a)^2$;
$Pr$, Prandtl number $\equiv \nu/\alpha$;
$q$, heat flux;
$r, \theta, \varphi$, toroidal coordinates;
$R$, non-dimensional radial coordinate;
$\Delta R, \Delta\theta$, mesh sizes in $R$- and $\theta$-directions;
$Re$, Reynolds number $\equiv 2aw_m/\nu$;
$Ro$, non-dimensional parameter representing the magnitude of the Coriolis force $\equiv a^2\Omega/\nu$;
$s$, arc length of tube axis $= b\varphi$;
$t$, temperature;
$\Delta t_2$, representative temperature $\equiv PraC_2$;
$T$, non-dimensional temperature $\equiv (t_w - t)/\Delta t_2$;
$u, v, w$, velocity components in $r$-, $\theta$- and $\varphi$-directions;

$U, V, W$, non-dimensional velocity components in $R$-, $\theta$- and $\varphi$-directions $\equiv au/v, av/v$ and $w/w_1$;
$w_1$, representative velocity in $\varphi$-direction $\equiv a^2C_1/\mu$;
$x', y', z'$, Cartesian coordinates;
$\alpha$, thermal diffusivity;
$\alpha_1, i, j, \ldots \alpha_5, i, j$, coefficients in finite difference equation;
$\beta$, volume expansion coefficient;
$\delta$, prescribed error for iterative process;
$\varepsilon$, ratio of mesh sizes $\equiv \Delta R/\Delta\theta$;
$\zeta$, vorticity;
$\eta$, quantity in equation (47);
$\mu$, viscosity;
$\nu$, kinematic viscosity;
$\rho$, density;
$\tau$, shearing stress;
$\psi$, stream function;
$\omega$, relaxation parameter;
$\Omega$, angular velocity.

Subscripts
$b$, bulk mean;
$i, j$, space subscripts of grid point in $R$- and $\theta$-directions;
$l$, local;
$m$, mean;
$s$, stationary straight circular tube;
$w$, wall;
$r, \varphi$, $r$- and $\varphi$-components.

## 1. INTRODUCTION

IN RECENT years it has become increasingly important to incorporate some cooling system into the design of rotary machines such as gas turbines, electric generators, motors, etc. An improvement in the thermal efficiency of a gas turbine can be effectively achieved by increasing the gas temperature at the inlet of turbine. However, the maximum temperature at which the present day materials for rotor blades insure the reliable operation of a gas turbine plant is approximately 850°C so that, if the inlet gas temperature exceeds this value, some cooling device is essential. Schmidt first proposed that this problem could be solved by the use of blades with holes drilled radially filled with some cooling substance. It is expected that this gives an extremely effective cooling, because the centrifugal acceleration can become of the order of $10^4g$. Many investigations of heat transfer inside these thermosyphon holes have been reported. These investigations were, however, conducted under the Earth's gravitational field, which differs from the rotational field in the presence of Coriolis forces which induce a secondary flow in a plane perpendicular to the main flow.

Further, the employment of some cooling device for electric generators are also of great importance to protect the insulating materials surrounding conductors, which are usually resistant against a high temperature up to 100–150°C for a reliable long-range operation. As a coolant, air was first used. It was then replaced by pressurized hydrogen which has a larger thermal capacity. The cooling is effected by pumping a coolant through hollow passages located inside the conductors or through axially located holes in the rotor drum. The hydrogen-cooling method makes it possible to construct a generator with the output of up to 250000 kW compared with the maximum output of 60000 kW for an air-cooled generator. Recently it has been attempted to employ water which is the most efficient coolant. The water-cooled generators have been in practice constructed in the Soviet Union, Switzerland, etc., and put into operation, though there are some technical difficulties encountered in sealing, strength, balancing of rotor, and insulation. It is estimated that this type of cooling method is capable of the maximum output of 750000 kW.

As a rotating geometry many configurations can be envisaged according to the shape and location of cooled components, i.e. (a) open thermosyphon, (b) closed thermosyphon, (c) straight tube rotating about a parallel axis, (d) straight tube rotating about a perpendicular axis, and (e) rotating curved tube. The first two,

(a) and (b), are the configurations attempted to be utilized for the cooling of gas turbine blades. The first and the last three, (a), (c), and (d) and (e), are the configurations encountered in cooling rotor drums and conductors of electric generator.

A remarkable characteristic of the flow and heat transfer in the rotational system of motion is the presence of centrifugal and Coriolis forces which induce a secondary flow in a plane perpendicular to the direction of main flow, and the flow and temperature fields are consequently three-dimensional. The secondary flow also arises, when a tube is curved, and enhances significantly the pressure drops and heat-transfer rates. In spite of the great practical importance and academic interest, the flow and heat transfer in rotating configurations are not yet sufficiently investigated, and little information is available for the design. Barua [1] has reported the theoretical analysis of the fully developed flow in a straight tube with circular cross section rotating about a perpendicular axis [the configuration (d)]. Morris [2] has presented the result of theoretical analysis for the asymptotic velocity and temperature distributions in the configuration (c) solved by a series expansion in terms of the rotational Rayleigh number. Humphreys *et al.* [3] also investigated experimentally the local and mean heat-transfer characteristics for air flowing turbulently in the entrance of a circular duct revolving about a parallel axis. Mori and Nakayama [4] have solved the same problem by Pohlhausen's method, and presented the pressure-drop and heat-transfer characteristics, which hold for a large angular velocity.

Compared with the problem in a rotating system the study on the flow-friction and heat transfer characteristics in curved stationary tubes has been fully made in conjunction with the application to heating and refrigerating plants. It was first treated theoretically by Dean [5, 6], who has solved the equations of flow by perturbation, and clarified that the flow field is controlled by the Dean number alone. Adler [7] made the extensive measurements of velocity distribution, and has found that the boundary-layer approximation holds for large values of the Dean number. He has also made a theoretical analysis by Pohlhausen's method, referring to the results of his measurements. By the same method Barua [8] has solved the flow field, and later Mori and Nakayama [9, 10] have reported the results of their theoretical analysis for both laminar and turbulent flows which are valid for large Dean numbers. The experimental investigations were made for turbulent flow and heat transfer by Ito [11], Seban and McLaughlin [12], Rogers and Mayhew [13], etc.

The investigation for the configuration (e) has been attempted by Ludwieg [14]. He has solved the boundary-layer equations by Pohlhausen's method for large values of the Dean number and rotational velocity for the fully developed laminar flow in a square tube, and obtained the friction factor which was verified by his experiment.

The object of the present analysis is to investigate theoretically the flow-friction and heat-transfer characteristics in curved circular tube rotating about the axis through the center of curvature [configuration (e)]. The governing equations are approximated by finite difference schemes and solved by iterative method under the conditions that the flow and temperature fields are fully developed, and the wall heat flux is uniform with peripherally uniform wall temperature. The results of computations are presented graphically for the temperature and velocity distributions, the streamlines and isothermals, and the local and mean Nusselt numbers and friction factors.

## 2. THEORETICAL ANALYSIS

### *Governing equations*

The geometrical configuration of the physical model for a rotating curved circular tube and its coordinate system are given in Fig. 1. The sense of the angular velocity vector is such that the direction of the axial velocity coincides with that of the rotational velocity. The cross section of the tube is perpendicular to the tube axis 0′0. For the convenience of the theoretical analysis the toroidal coordinate system $(r, \theta, \varphi)$ is employed, and the governing equations are described in terms of this coordinate system instead of the Cartesian coordinate system $(x', y', z')$. The velocity components in the $r$-, $\theta$- and $\varphi$-directions are denoted by $u, v$ and $w$ respectively. The parts of the tube wall are termed the inner, outer, upper and lower walls for the convenience of explanations of computational results. The horizontal and vertical center lines, along which the axial velocity and temperature distributions will be presented in a graphical form, are also indicated in the figure.

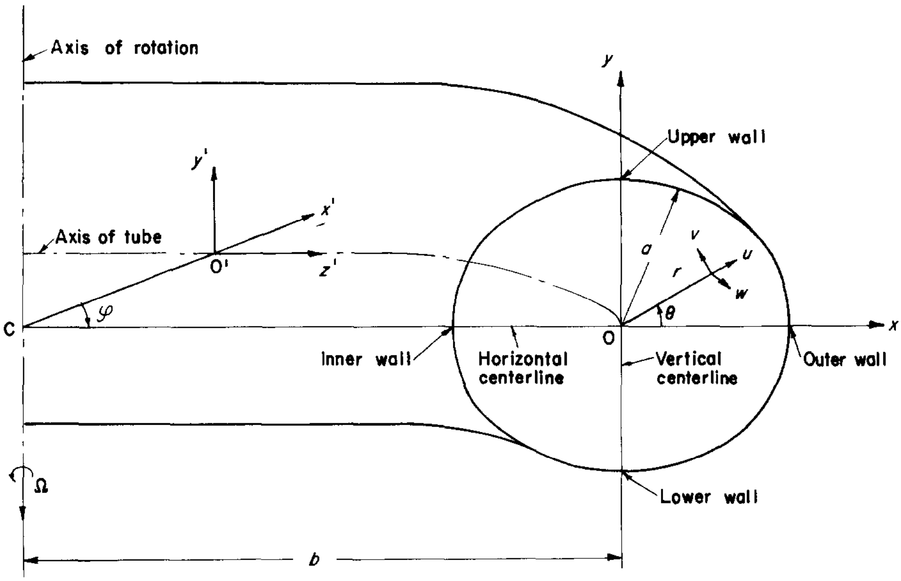


FIG. 1. Toroidal coordinate system.

The flow is assumed to be laminar and, with the exception of density, the physical properties are taken to be constant. The axial velocity is so low that there is no energy dissipation due to friction, and no heat source is present within the cooling fluid. The gravitational force is neglected compared with the centrifugal force due to rotation. The rotational acceleration is usually of the order of $10^3$–$10^4 g$ for the rotary machines which we are concerned with so that the elimination of gravitational force term apparently causes no significant errors. The detailed derivation of the governing equations which describe the aforementioned physical model is given in [15]. They are, however, too complicated to solve so that some additional assumptions will be made to simplify them. First, we consider a special case that the radius of curvature $b$ is much larger than the radius of tube $a$, i.e. $B \gg 1$. This is justified by the fact that $B$ is approximately 50 at the actual situations of application. Further, the mean friction factors $f$ and Nusselt numbers $Nu$ for both the exact equations and the simplified equations with $B \gg 1$ were computed and compared in [15] in the case of a square tube, varying $B$ from 5 to 500 which covers the range of practical interest. The result shows that there is substantially no difference between the two solutions in the vicinity of $B = 50$, and at $B = 5$ the simplified solutions for $f$ and $Nu$ are respectively 6 and 2 per cent lower than the exact solutions, while at $B = 500$ they are 3 and 2 per cent higher. Consequently, it can be anticipated that this simplification does not cause intolerable errors. With this assumption the term $r \cos\theta$ is to be ignored compared with $b$. Further, all the terms which have $b$ in their denominator are negligible in comparison with those which have $r$ in their denominator or those of derivatives with respect to $r$. However, the centrifugal force term $w^2/b$ should be retained, since the axial velocity $w$ is much larger than the velocity components of secondary flow $u$, $v$.

Next, we deal with the hydrodynamically and thermally fully developed flow regime, where the axial pressure and temperature gradients become constant, i.e. $\partial p/\partial s = -C_1$ and $\partial t/\partial s = C_2$. Further, the velocity and temperature distributions maintain a similar form in the axial direction and become independent of the coordinate $\varphi$.

Before we introduce the simplified equations, we modify the centrifugal force terms. The density varies with temperature according to the relation

$$\rho = \rho_w + \rho_w \beta(t_w - t) \approx \rho_w + \rho\beta(t_w - t), \quad (1)$$

since $\rho_w \approx \rho$. In general the volume expansion coefficient $\beta$ is a function of temperature, and the temperature dependence of $\beta$ is not necessarily negligible for water. However, it was found in [15] that the differences of $f$ and $Nu$ between the cases of variable and constant $\beta$ were approximately 0·6 and 2 per cent respectively. This discrepancy is tolerable for the industrial applications so that $\beta$ is taken to be constant in the present analysis. Therefore, the rotational centrifugal force per unit volume is rewritten in the form, noting that the acceleration of centrifugal force is $f_c = b\Omega^2$ and using equation (1),

$$\rho b \Omega^2 \approx \rho_w f_c + \rho f_c \beta(t_w - t). \quad (2)$$

In addition we introduce the modified pressure $p'$ such that

$$p' = p - \rho_w f_c r \cos\theta. \quad (3)$$

The second term on the right-hand side of equation (3) is a centrifugal force acting in the $x$-direction and balanced with the pressure gradient so that it makes no contribution to the motion of fluid in tube. With these assumptions, we obtain the following simplified equations

$$\frac{\partial(ru)}{\partial r} + \frac{\partial v}{\partial \theta} = 0, \quad (4)$$

$$u\frac{\partial u}{\partial r} + v\frac{\partial u}{r\partial\theta} - \frac{v^2}{r} - \cos\theta\frac{w^2}{b} - 2\Omega\cos\theta\, w - f_c\beta\cos\theta(t_w - t) = -\frac{1}{\rho}\frac{\partial p'}{\partial r} - \nu\frac{\partial}{r\partial\theta}\left(\frac{\partial v}{\partial r} + \frac{v}{r} - \frac{\partial u}{r\partial\theta}\right), \quad (5)$$

$$u\frac{\partial v}{\partial r} + v\frac{\partial v}{r\partial\theta} + \frac{uv}{r} + \sin\theta\frac{w^2}{b} + 2\Omega\sin\theta w + f_c\beta\sin\theta(t_w - t) = -\frac{1}{\rho}\frac{\partial p'}{r\partial\theta} + \nu\frac{\partial}{\partial r}\left(\frac{\partial v}{\partial r} + \frac{v}{r} - \frac{\partial u}{r\partial\theta}\right), \quad (6)$$

$$u\frac{\partial w}{\partial r} + v\frac{\partial w}{r\partial\theta} + 2\Omega(u\cos\theta - v\sin\theta) = \frac{1}{\rho}C_1 + \nu\left(\frac{\partial^2 w}{\partial r^2} + \frac{1}{r}\frac{\partial w}{\partial r} + \frac{\partial^2 w}{r^2\partial\theta^2}\right), \quad (7)$$

$$u\frac{\partial t}{\partial r} + v\frac{\partial t}{r\partial\theta} + C_2 w = \alpha\left(\frac{\partial^2 t}{\partial r^2} + \frac{1}{r}\frac{\partial t}{\partial r} + \frac{\partial^2 t}{r^2\partial\theta^2}\right), \quad (8)$$

which are subject to the boundary conditions

$$u = v = w = 0, \qquad t = t_w \text{ at wall.} \quad (9)$$

In order to non-dimensionalize the governing equations thus obtained, we introduce the following non-dimensional variables

$$U = \frac{au}{\nu}, \quad V = \frac{av}{\nu}, \quad W = \frac{w}{w_1},$$

$$P = \frac{p'}{\rho(\nu/a)^2}, \quad T = \frac{t_w - t}{\Delta t_2}, \quad R = \frac{r}{a}. \quad (10)$$

Further, we attempt to alter the non-dimensional equations to facilitate the numerical computation. The equation of continuity is identically satisfied by the stream function $\psi$

$$U = \frac{\partial \psi}{R \partial \theta}, \qquad V = -\frac{\partial \psi}{\partial R}. \tag{11}$$

We introduce the vorticity of secondary flow $\zeta$

$$\zeta = \frac{\partial V}{\partial R} + \frac{V}{R} - \frac{\partial U}{R \partial \theta}. \tag{12}$$

Substitution of equations (11) into (12) yields the equation of stream function

$$\nabla^2 \psi = -\zeta. \tag{13}$$

The equation of vorticity is derived by eliminating the irrelevant pressure terms from the two equations of momentum in the $R$- and $\theta$-directions, and is given by

$$\begin{aligned}\nabla^2 \zeta &= U \frac{\partial \zeta}{\partial R} + V \frac{\partial \zeta}{R \partial \theta} \\ &+ \tfrac{1}{2} K_1^2 \left( \cos\theta \, W \frac{\partial W}{R \partial \theta} + \sin\theta \, W \frac{\partial W}{\partial R} \right) + \\ &(\surd B) Ro K_1 \left( \cos\theta \frac{\partial W}{R \partial \theta} + \sin\theta \frac{\partial W}{\partial R} \right) \\ &+ Gr_2 \left( \cos\theta \frac{\partial T}{R \partial \theta} + \sin\theta \frac{\partial T}{\partial R} \right).\end{aligned} \tag{14}$$

The equations of axial momentum and energy are to be rewritten in the form

$$\begin{aligned}\nabla^2 W &= U \frac{\partial W}{\partial R} + V \frac{\partial W}{R \partial \theta} + \frac{4Ro}{(\surd B) K_1} \\ &\times (U \cos\theta - V \sin\theta) - 1,\end{aligned} \tag{15}$$

$$\nabla^2 T = Pr \left( U \frac{\partial T}{\partial R} + V \frac{\partial T}{R \partial \theta} \right) - \frac{(\surd B) K_1}{2} W. \tag{16}$$

Equations (11) and (13)–(16) are the final system of equations to be solved, and are subject to the boundary conditions

$$U = V = \psi = \frac{\partial \psi}{\partial R} = W = T = 0 \text{ at } R = 1. \tag{17}$$

Since it is readily found that $U$, $W$ and $T$ are symmetric, and $V$, $\psi$ and $\zeta$ are anti-symmetric with respect to the horizontal centerline, the boundary conditions are altered to

$$U = V = \psi = \frac{\partial \psi}{\partial R} = W = T = 0 \quad \text{at} \quad R = 1 \text{ for } 0 \leqslant \theta \leqslant \pi, \tag{18}$$

$$\frac{\partial U}{\partial \theta} = \frac{\partial W}{\partial \theta} = \frac{\partial T}{\partial \theta} = V = \psi = \zeta = 0 \quad \text{at} \quad \theta = 0, 2\pi \text{ for } 0 \leqslant R \leqslant 1, \tag{19}$$

and it suffices to consider the upper half of the cross section alone owing to symmetry.

*Finite difference representation*

All the governing equations are to be expressed in the following general form, using a dummy function $F$ which represents either one of the dependent variables

$$\nabla^2 F + D \frac{\partial F}{\partial R} + E \frac{\partial F}{\partial \theta} + C = 0. \tag{20}$$

$D$ and $E$ are either $-U$, $-V/R$ or $-PrU$, $-PrV/R$ respectively, and $C$ is a source term. The radial coordinate is divided into $M$ segments with the step size $\nabla R = 1/M$, while the angular coordinate is divided into $N$ segments with the step size $\Delta\theta = \pi/N$. An arbitrary grid point in the domain is denoted by $(i, j)$, and the derivatives in equation (20) are approximated by appropriate finite difference schemes. To the non-linear inertia terms we apply the modified one-sided difference scheme utilized by Spalding *et al.* [16] in order to assure stability, i.e.

$$\begin{aligned}\left( D \frac{\partial F}{\partial R} \right)_{i,j} &\approx \frac{D_{i,j} + |D_{i,j}|}{2\Delta R} F_{i+1,j} \\ &- \frac{|D_{i,j}|}{\Delta R} F_{i,j} - \frac{D_{i,j} - |D_{i,j}|}{2\Delta R} F_{i-1,j} + O(\Delta R),\end{aligned} \tag{21}$$

$$\left(E\frac{\partial F}{\partial \theta}\right)_{i,j} \approx \frac{E_{i,j}+|E_{i,j}|}{2\Delta\theta}F_{i,j+1} - \frac{|E_{i,j}|}{\Delta\theta}F_{i,j} - \frac{E_{i,j}-|E_{i,j}|}{2\Delta\theta}F_{i,j-1} + 0(\Delta\theta). \quad (22)$$

The Laplacian operator is replaced by the central difference scheme

$$\nabla^2 F \approx \frac{F_{i+1,j} - 2F_{i,j} + F_{i-1,j}}{\Delta R^2} + \frac{1}{R_i}\cdot\frac{F_{i+1,j} - F_{i-1,j}}{2\Delta R} + \frac{F_{i,j+1} - 2F_{i,j} + F_{i,j-1}}{\Delta\theta^2} + 0(\Delta R^2, \Delta\theta^2). \quad (23)$$

Approximating the differential equation (20) by the finite difference schemes (21)–(23) and solving for $F_{i,j}$, we get

$$F_{i,j} \approx \alpha_{1,i,j}F_{i+1,j} + \alpha_{2,i,j}F_{i-1,j} + \alpha_{3,i,j}F_{i,j+1} + \alpha_{4,i,j}F_{i,j-1} + \alpha_{5,i,j}C_{i,j}, \quad (24)$$

where

$$\alpha_{1,i,j} = \left\{1 + \Delta R/2R_i + (D_{i,j} + |D_{i,j}|)\frac{\Delta R}{2}\right\}\Big/R_{i,j},$$

$$\alpha_{2,i,j} = \left\{1 - \Delta R/2R_i - (D_{i,j} - |D_{i,j}|)\frac{\Delta R}{2}\right\}\Big/R_{i,j},$$

$$\alpha_{3,i,j} = \left\{\varepsilon^2/R_i^2 + (E_{i,j} + |E_{i,j}|)\frac{\varepsilon\Delta R}{2}\right\}\Big/R_{i,j}, \quad (25)$$

$$\alpha_{4,i,j} = \left\{\varepsilon^2/R_i^2 - (E_{i,j} - |E_{i,j}|)\frac{\varepsilon\Delta R}{2}\right\}\Big/R_{i,j},$$

$$\alpha_{5,i,j} = \Delta R^2/R_{i,j}$$

with $R_{i,j} = 2(1 + \varepsilon^2/R_i^2) + (|D_{i,j}| + |E_{i,j}|\varepsilon)\Delta R$ and $\varepsilon = \Delta R/\Delta\theta$. The coefficients $D_{i,j}$, $E_{i,j}$ and the source term $C_{i,j}$ take on specific forms for each dependent variable, but their presentation is abbreviated. Equations (11) are approximated by

$$U_{i,j} \approx \frac{\psi_{i,j+1} - \psi_{i,j-1}}{R_i 2\Delta R}\cdot\varepsilon + 0(\Delta\theta^2), \quad (26)$$

$$V_{i,j} \approx -\frac{\psi_{i+1,j} - \psi_{i-1,j}}{2\Delta R} + 0(\Delta R^2). \quad (27)$$

The boundary conditions (18) and (19) become in the finite difference form

$$U_{M+1,j} = V_{M+1,j} = \psi_{M+2,j} - \psi_{M,j} = W_{M+1,j} = T_{M+1,j} = 0, \quad (28)$$

$$U_{i,2} - U_{i,0} = W_{i,2} - W_{i,0} = T_{i,2} - T_{i,0} = V_{i,1} = \psi_{i,1} = \zeta_{i,1} = 0, \quad (29)$$

$$U_{i,N+2} - U_{i,N} = W_{i,N+2} - W_{i,N} = T_{i,N+2} - T_{i,N} = V_{i,N+1} = \psi_{i,N+1} = \zeta_{i,N+1} = 0, \quad (30)$$

where the values at grid points outside the domain are eliminated by the use of equation (24) applied to a corresponding boundary point.

The wall vorticity is computed from the stream function by the Dorfman–Romanenko's approximation [17]. Applying the equation of stream function (13) to the wall $i = M + 1$, and considering the boundary conditions (18), we obtain the vorticity at wall

$$\zeta_{M+1,j} = -\left(\frac{\partial^2\psi}{\partial R^2}\right)_{M+1,j}. \quad (31)$$

The stream function at $i = M$ is developed into the Taylor series about the point $i = M + 1$ as

$$\psi_{M,j} \approx \psi_{M+1,j} - \left(\frac{\partial\psi}{\partial R}\right)_{M+1,j}\Delta R + \left(\frac{\partial^2\psi}{\partial R^2}\right)_{M+1,j}\frac{\Delta R^2}{2!} - \left(\frac{\partial^3\psi}{\partial R^3}\right)_{M+1,j}\frac{\Delta R^3}{3!} + 0(\Delta R^4). \quad (32)$$

Since $\psi_{M+1,j} = (\partial\psi/\partial R)_{M+1,j} = 0$, equation (32) becomes, using equation (31)

$$\psi_{M,j} \approx -\frac{\Delta R^2}{2}\zeta_{M+1,j} - \frac{\Delta R^3}{6}\left(\frac{\partial^3\psi}{\partial R^3}\right)_{M+1,j} + 0(\Delta R^4). \quad (33)$$

Differentiation of equation (13) with respect to

$R$ yields the following relation at $i = M + 1$

$$\left(\frac{\partial \zeta}{\partial R}\right)_{M+1,j} = -\left(\frac{\partial^3 \psi}{\partial R^3}\right)_{M+1,j} - \left(\frac{1}{R}\frac{\partial^2 \psi}{\partial R^2}\right)_{M+1,j}$$

$$= -\left(\frac{\partial^3 \psi}{\partial R^3}\right)_{M+1,j} + \zeta_{M+1,j}. \quad (34)$$

The derivative on the left-hand side of equation (34) is replaced by the forward difference. Then solving equation (34) for the third derivative of stream function at $i = M + 1$, and substituting it into equation (32), we finally obtain the wall vorticity

$$\zeta_{M+1,j} \approx -\frac{3}{\Delta R^2(1 + \Delta R/2)}\psi_{M,j} - \frac{1}{2(1 + \Delta R/2)}\zeta_{M,j} + 0(\Delta R^2). \quad (35)$$

The above vorticity was not used explicitly in the iterative process to remove a cause of instability. It was omitted by the use of equation (24) for the vorticity at wall, and was computed from equation (35), after solutions have converged.

The governing equations have a singular point at the center $R = 0$ so that the finite difference equation (24) ceases to apply there. Since the stream function and vorticity are independent of $\theta$, the boundary conditions (19) for them holds identically at the center, i.e.

$$\psi_{1,j} = \zeta_{1,j} = 0. \quad (36)$$

The rest of the dependent variables are determined by extrapolation. The parabolic extrapolation formula from the values at the neighbouring three successive points gives

$$F_{1,j} = 3F_{2,j} - 3F_{3,j} + F_{4,j}. \quad (37)$$

The iterative procedure was employed to obtain the solutions for equation (24). To increase the convergence rate the overrelaxation method was used, and the relaxation parameter was evaluated from $\omega = 2[1 + \sqrt{(1 - \eta)}]/\eta$ with $\eta = (\cos \pi/M + \cos \pi/N)/2$. To the iteration of vorticity, however, the underrelaxation method was applied so that the fluctuation of vorticity during the iteration is small enough for instability not to emerge. The iterative computation was terminated, when the relative error of solutions became less than some preassigned small quantity $\delta$. It was found from the preliminary computations that $M = N = 24$ secured a sufficient accuracy correct up to three significant figures with $\delta = 0{\cdot}001$ for relatively small values of the non-dimensional parameters. However, for $Pr > 1{\cdot}3$, $Ro > 30$, $Gr_2 > 3000$ and $K_1 > 300$, $M = N = 36$ was used with $\delta = 0{\cdot}001$ to obtain convergent solutions with sufficient accuracy. The underrelaxation parameter was varied from 0·15 to 0·5 according to the magnitude of the non-dimensional parameters.

*Evaluation of* f *and* Nu

The mean friction factor $f$ is defined by

$$-\,\mathrm{d}p = f \cdot \frac{\mathrm{d}s}{2a} \cdot \tfrac{1}{2}\rho w_m^2, \quad (38)$$

which is solved for $f$ as

$$f = \frac{8}{(\sqrt{B})K_1 W_m} = \frac{8}{ReW_m}, \quad (39)$$

or

$$\frac{f \cdot Re}{f_s \cdot Re} = \frac{1}{8W_m} \quad (40)$$

The mean Nusselt number is obtained from the heat balance equation. The increase of fluid enthalpy per the tube length $\mathrm{d}s$ is equal to the heat supplied from wall of length $\mathrm{d}s$ by convection so that

$$\rho c_p C_2 \,\mathrm{d}s\, \pi a^2 w_m = 2\pi a \,\mathrm{d}s\, h(t_w - t_b). \quad (41)$$

The mean Nusselt number is defined as $Nu$ $2ah/k$, which is rewritten in the form, using equation (41) after some rearrangements

$$Nu = \frac{(\sqrt{B})K_1}{2T_b}, \text{ or } \frac{Nu}{Nu_s} = \frac{11}{96} \cdot \frac{(\sqrt{B})K_1}{T_b}. \quad (42)$$

The wall shearing stress acting in the axial direction is

$$(\tau_{r,\varphi})_{r=a} = -\mu\left(\frac{\partial w}{\partial r}\right)_{r=a} \quad (43)$$

Non-dimensionalizing the shearing stress by the dynamic pressure $\frac{1}{2}\rho w_m^2$, and dividing it by $f_s . Re = 64$, we have

$$\frac{(f_l)_{r=a} . Re}{f_s . Re} = -\frac{1}{16W_m}\left(\frac{\partial W}{\partial R}\right)_{R=1}. \tag{44}$$

The first derivative is represented by the four-point approximation

$$\left(\frac{\partial W}{\partial R}\right)_{R=1} \approx \frac{-11W_{M+1,j} + 18W_{M,j} - 9W_{M-1,j} + 2W_{M-2,j}}{6\Delta R} + 0(\Delta R^3). \tag{45}$$

Noting $W_{M+1,j} = 0$, substitution of equation (45) into (44) yields

$$\frac{(f_l)_{r=a} . Re}{f_s . Re} \approx \frac{1}{96W_m} \times \frac{18W_{M,j} - 9W_{M-1,j} + 2W_{M-2,j}}{\Delta R} \tag{46}$$

The $r$-component of local heat flux at wall directed toward the inside of tube is given by

$$(q)_{r=a} = k\left(\frac{\partial t}{\partial r}\right)_{r=a} = h_l(t_w - t_b). \tag{47}$$

The local Nusselt number is defined as $Nu_l = 2ah_l/k$. Dividing $Nu_l$ by $Nu_s = 48/11$ and applying the four-point approximation to the derivative of temperature, we obtain with $T_{M+1,j} = 0$

$$\frac{Nu_l}{Nu_s} \approx \frac{11}{48T_b} \times \frac{18T_{M,j} - 9T_{M-1,j} + 2T_{M-2,j}}{\Delta R} \tag{48}$$

### 3. RESULTS AND DISCUSSION

A great difference between a circular tube and rectangular tubes for which the results of computations are presented in [15] is seen in the formation of secondary flow. The secondary flow occurs in the plane perpendicular to the tube axis so that the shape of tube cross section is a determining factor of its rise. It also affects the pattern and intensity of secondary current. Since the circular cross section has geometrically a less resistance against the current, the secondary flow occurs more readily, and its effects on the friction factor and the Nusselt number appear at much smaller values of the non-dimensional parameters. There is also no corner effect which produces stagnant regions at corners of cross section, and reduces greatly the flow friction and heat transfer.

There are five non-dimensional parameters, $B$, $Pr$, $Ro$, $Gr_2$ and $K_1$, and computations are required for an extremely large number of cases to grasp the entire characteristics. Considering the economy, therefore, computations were made such that the standard values of the parameters, $B = 50$, $Pr = 0{\cdot}7$, $Ro = 1$, $Gr_2 = 10$ and $K_1 = 10$ were chosen, and, to see the effects of one parameter, the rest of the parameters were fixed at the standard values. Since the effects of $B$ was found to be minor from the computations for rectangular tubes in [15], it was fixed at 50. Further, the additional standard values, $B = 50$, $Ro = 10$, $Gr_2 = 10$ and $K_1 = 100$ were selected to see the effects of $Pr$ more clearly. The results of computations are presented for the axial velocity and temperature distributions, the streamlines and isothermals, the local friction factors and Nusselt numbers, and the mean friction factors and Nusselt numbers. However, it is lengthy to describe the effects of all the parameters on the flow and heat-transfer characteristics so that the descriptions here will be constricted to the effects of $Ro$ alone except those on the mean friction factors and Nusselt numbers, provided that the effect of $Pr$ on the mean characteristics is eliminated. The complete presentation of the results is made in [15].

Figures 2 and 3 show the effects of $Ro$ on the axial velocity and temperature distributions. The solid, dotted and one-dotted lines represent the curves for $Ro = 1$, 10 and 70 respectively. The Coriolis forces have the components in the plane of secondary flow and in the $\varphi$-direction. The resultant force of the former components,

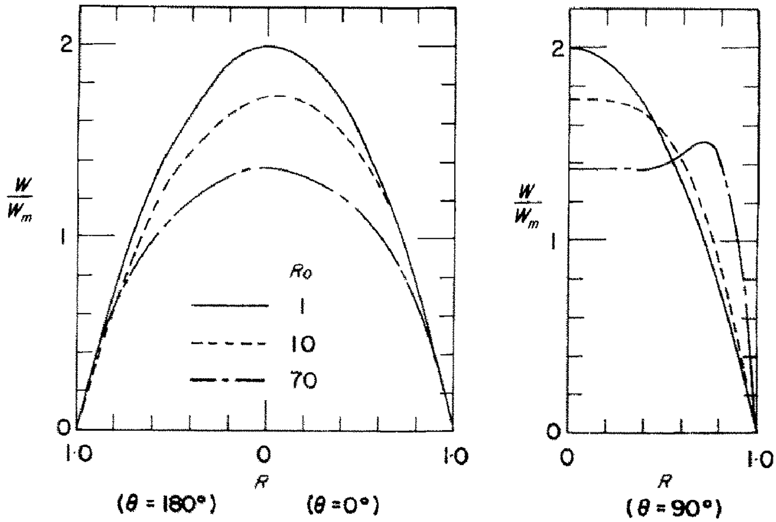


FIG. 2. Variation of axial velocity distribution with $Ro$ ($B = 50$, $Pr = 0{\cdot}7$, $Gr_2 = 10$, $K_1 = 10$).

which is proportional to the axial velocity $w$, is directed outward from the axis of rotation, and induces the secondary flow. The latter component is proportional to the velocity of the secondary flow, and deccelerates the main flow in the central region so that the axial velocity distribution is flattened with the increase in $Ro$. In the vicinity of the upper wall, however, the fluid is accelerated by this component because the direction of secondary current is reversed. In consequence the Coriolis force together with the inertia force causes the increase in the axial velocity there as shown in the right figure for the velocity distribution along the vertical center-line. The velocity distributions are almost symmetric about the center owing to the property of the Coriolis forces which tend to restore the flow system to an equilibrium state. The variation of temperature distribution is less marked. It is due to the fact that the relatively strong secondary

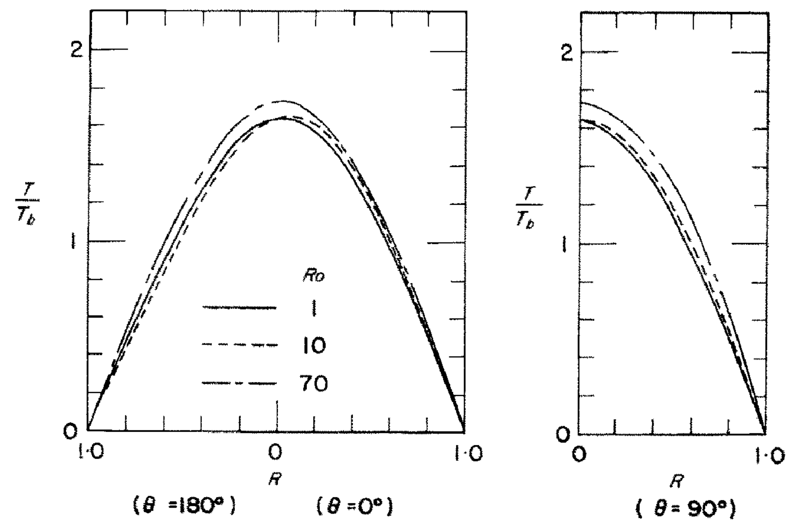


FIG. 3. Variation of temperature distribution with $Ro$ ($B = 50$, $Pr = 0{\cdot}7$, $Gr_2 = 10$, $K_1 = 10$).

current is constrained to the close vicinity of the upper and lower walls, and it is weak in the broad central core. The heat convected by the secondary current is so small in the central region that the heat is supplied by conduction which results in temperature gradient rather than flattening. The conducted heat is carried away by the main flow by convection. Since the convected heat is axisymmetric owing to the symmetry of the axial velocity, the temperature distributions are also symmetric about the center.

The streamlines and isothermals were obtained by interpolation from the stream function and temperature distributions respectively. Since they are symmetric about the horizontal centerline, the former are plotted in the upper half plane and the latter in the lower half plane. The three streamlines are drawn such that they pass either one of the points $R \approx 0{\cdot}1$, $0{\cdot}2$ and $0{\cdot}33$ at $\theta = 90°$, and a value of stream function for each streamline is specified so as to be able to assess the flow rate and intensity of secondary flow. The four isothermals are illustrated for $T/T_b \approx 0{\cdot}3$. $0{\cdot}7$, $1{\cdot}0$ and $1{\cdot}5$ so that the density of isothermals indicates the steepness of temperature gradient. The axis of rotation is located on the left-hand side of the tube cross section so that the circular secondary current flows counterclockwise in the upper half plane.

Figures 4 and 5 show the streamlines and isothermals for the standard values ($Ro = 1$) and $Ro = 70$ respectively. For $Ro = 1$ the effect of the Coriolis forces is negligibly small. The secondary flow must be governed mainly by the buoyancy and centrifugal forces, and accordingly the pattern of streamlines are somewhat shifted toward the upper wall. For $Ro = 70$ an essentially different flow field is formed. The flow is uniform over a broad central region which occupies approximately a half of cross sectional area. However, the current velocity is extremely low as seen from the values of stream function. This is attributable to the restoring property of the Coriolis forces which push back the main flow and flatten the axial velocity distribution. The

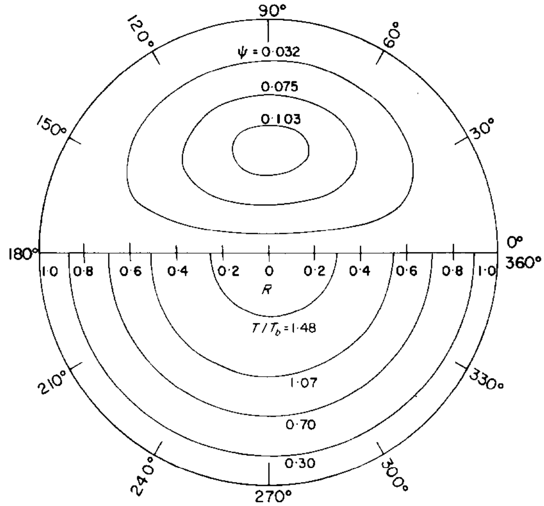


FIG. 4. Streamlines and isothermals for standard values of parameters
($B = 50$, $Pr = 0{\cdot}7$, $Ro = 1$, $Gr_2 = 10$, $K_1 = 10$).

returning secondary current is forced to flow through a narrow passage in the close vicinity of the upper wall owing to the broadening of the central core. The streamlines are dense there, but there is not a great increase in velocity because the secondary flow itself is not very strong. The isothermals tend to be displaced at first. The temperature gradient is, therefore, steep at the outer wall, and is gradual at the inner wall.

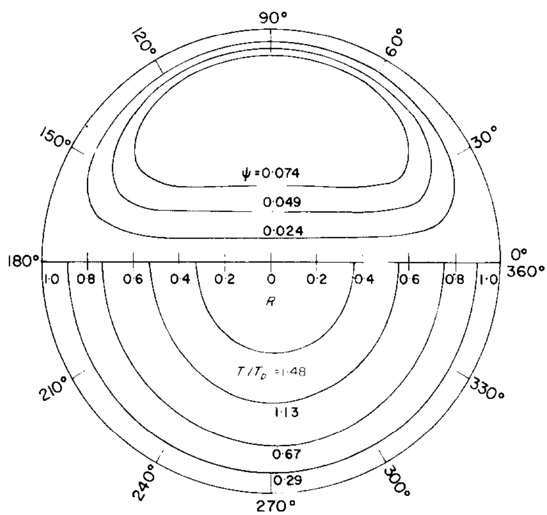


FIG. 5. Streamlines and isothermals for $Ro = 70$
($B = 50$, $Pr = 0{\cdot}7$, $Gr_2 = 10$, $K_1 = 0$).

Further increase of $Ro$ results in the symmetric pattern of isothermals about the vertical center line. The temperature gradient at the lower wall increases somewhat because of the relatively strong secondary current there.

The results of the local friction factors and Nusselt numbers are plotted against the angle $\theta$. They are presented in reference to those for a stationary straight circular tube to see their relative increase and variation. In order to observe the effect of a non-dimensional parameter, the local friction factors and Nusselt numbers are computed for its three values with the rest of the parameters fixed at the standard values, and are represented by the solid, dotted and one-dotted lines respectively in the increasing order of magnitude of the parameter.

Figure 6 show the local friction factors and Nusselt numbers when $Ro$ is varied. $Ro$ has a peculiar effect which is typical of the Coriolis forces. The Coriolis force in the axial direction opposes the main flow, and flattens the axial velocity distribution. The larger the axial velocity, the larger the opposing force so that the central core with uniform secondary flow and constant axial velocity is formed, and, moreover, the flow field becomes symmetric about the vertical centerline. Consequently the distribution of the local friction factor is also symmetric about $\theta = 90°$. Since the Coriolis force acting on the returning secondary current in the vicinity of the upper wall causes the axial velocity and accordingly its gradient to increase. It results in the increase of friction factor at $\theta = 90°$, and an appreciable increase is seen for $Ro = 70$. The effect on the Nusselt number is on the other hand less pronounced, though the variation of the Nusselt number with $\theta$ is similar to that of the friction factor. The maximum value is only 1·5 for $Ro = 70$, while that of the friction factor is as large as almost 3·0.

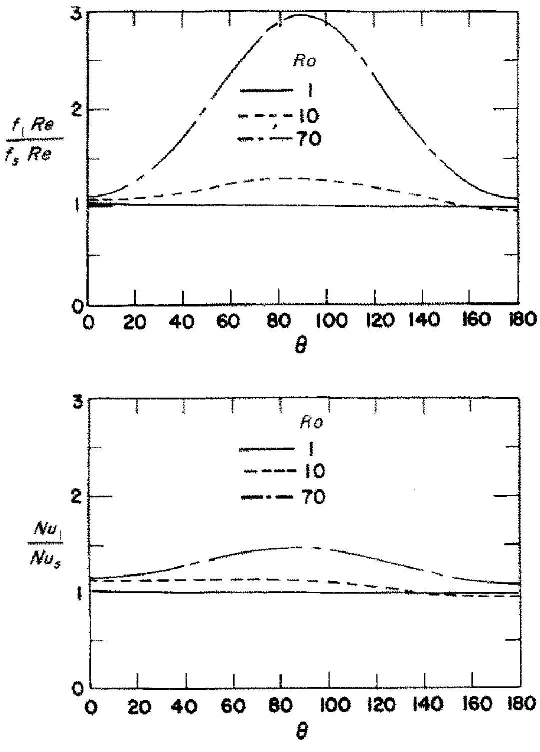


FIG. 6. Variation of local friction factor and Nusselt number with $Ro$
($B = 50$, $Pr = 0{\cdot}7$, $Gr_2 = 10$, $K_1 = 10$).

The mean friction factors $f$ and Nusselt numbers $Nu$ are plotted on semi-log scale against the non-dimensional parameters in the form of the ratio to those for a stationary straight circular tube $f_s$ and $Nu_s$. $f_s \cdot Re$ and $Nu_s$ are known to be 64 and 48/11 respectively for the fully developed laminar flow with constant wall heat flux. The non-dimensional parameters are varied as $Ro = 1$–$100$, $Gr_2 = 100$–$10000$ and $K_1 = 10$–$1000$, while $B$ is fixed at 50 because its effects are minor.

Figure 7 is the mean friction factor and Nusselt number against $Ro$, which are represented by the solid and dotted lines respectively. As it has

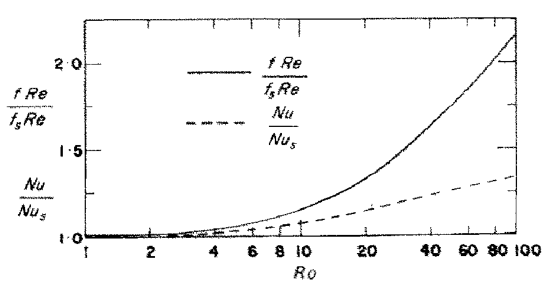


FIG. 7. Mean friction factor and Nusselt number vs. $Ro$
($B = 50$, $Pr = 0{\cdot}7$, $Gr_2 = 10$, $K_1 = 10$).

been pointed out before, the geometrical resistance against the secondary current is smaller for circular cross section. Consequently the effect of $Ro$ becomes evident at a smaller value $Ro \approx 2$ than for rectangular cross section $Ro \approx 10$. Moreover, the rate of increase is much larger. In the case of $f$, $f \, . \, Re/(f_s \, . \, Re)$ has almost the same value at $Ro = 10$ for both cases, but at $Ro = 100$ it is 1·5 for rectangular cross section, while it reaches as high as 2·15 for circular cross section. The increase in $f$ is more pronounced, because the Coriolis force acts as a resistant force against the main flow, and $f$ tends to asymptotically increase in proportion to $Ro^{\frac{1}{4}}$. The heat transfer is less enhanced by the Coriolis forces, and its asymptotic behaviour is such that $Nu$ is proportional to $Ro^{1/12}$ as in the case of rectangular cross section.

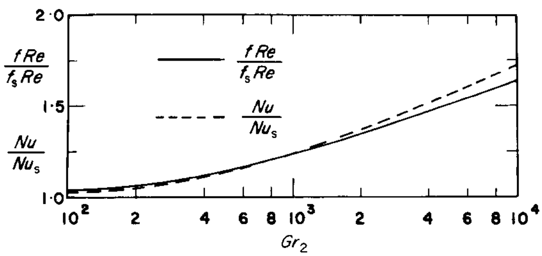


FIG. 8. Mean friction factor and Nusselt number vs. $Gr_2$ ($B = 50$, $Pr = 0{\cdot}7$, $Ro = 1$, $K_1 = 10$).

Figure 8 shows the plot of the mean friction factor and Nusselt number against $Gr_2$. The effect of secondary flow due to $Gr_2$ commences to become significant at $Gr_2 \approx 100$ compared with $Gr_2 \approx 1000$ for rectangular cross section. On the contrary to $Ro$ the increase rate of $Nu$ due to $Gr_2$ is higher than that of $f$, and $Nu/Nu_s$ exceeds $f \, . \, Re/(f_s \, . \, Re)$ at $Gr_2 \approx 1000$. For large $Gr_2$, $f$ and $Nu$ are proportional to $Gr_2^{1/9}$ and $Gr_2^{1/7}$ respectively. These results agree exactly with those of Mori and Makayama [8] for a circular tube rotating about a parallel axis.

Figure 9 shows the mean friction factor and Nusselt number against $K_1$. The effect of $K_1$ appears at $K_1 \approx 100$, which is the same value

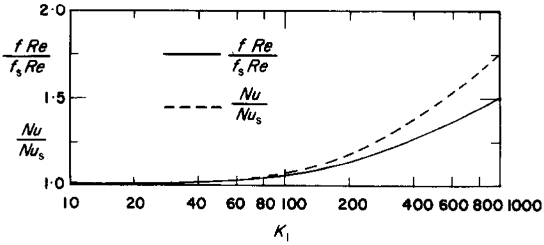


FIG. 9. Mean friction factor and Nusselt number vs. $K_1$ ($B = 50$, $Pr = 0{\cdot}7$, $Ro = 1$, $Gr_2 = 10$).

as for rectangular cross section. However, the increase rate of $f$ and $Nu$ is larger for circular cross section. The centrifugal force furthers heat transfer more than flow resistance as the buoyancy force does. $Nu$ increases at the same rate as $f$ up to about $K_1 = 100$, and more rapidly thereafter. The extrapolated behaviour is such that $f$ and $Nu$ vary proportionally to $K_1^{1/6}$ and $K_1^{1/4}$ respectively. For a stationary curved circular tube, however, both of them increase at the rate of $K_1^{1/2}$.

## 4. CONCLUSIONS

The problem treated in the present theoretical analysis is the flow and heat transfer in a curved circular tube rotating about the axis through the center of curvature. The flow-friction and heat-transfer characteristics are determined by the five non-dimensional parameters, the radius ratio $B$, the Prandtl number $Pr$, the parameter $Ro$, which represents the effects of the Coriolis forces, the Grashof number $Gr_2$ and the Dean number $K_1$. The governing equations are solved by finite difference method by the use of iterative procedure, and the results of computations are presented graphically for the axial velocity and temperature distributions, the streamlines and isothermals, the local friction factors and Nusselt numbers and the mean friction factors and Nusselt numbers. The evaluation of the above flow and heat-transfer characteristics is made, varying one of the non-dimensional parameters with the rest of the parameters fixed at the standard values which are $B = 50$, $Pr = 0{\cdot}7$, $Ro = 1$, $Gr_2 = 10$ and $K_1 = 10$. $B$ is, however, fixed at 50, since its effects on the flow and heat-transfer characteristics are minor. Due to the excessive length, the presentation and discussion are confined to the effects of $Ro$ alone on the flow and heat-transfer characteristics except those on the mean $f$ and $Nu$, provided that the effect of $Pr$ on the mean characteristics is abbreviated.

The formation and intensity of secondary flow is characteristic of each non-dimensional parameter. $Pr$ exercises substantially no effect, though the intensity of secondary flow tends to decrease very slightly. $Ro$ creates a broad central core where a uniform and rather weak secondary current flows, but a considerably strong returning current arises in the immediate vicinity of the upper and lower walls. The effect of $Gr_2$ is somewhere between those of $Ro$ and $K_1$. The secondary flow is strong not only in the central region but also in the neighbourhood of the upper and lower walls. $K_1$ induces a strong current along the horizontal centerline, which, however, decreases rapidly toward the upper or lower wall.

The friction factor $f$ and the Nusselt number $Nu$ are also affected characteristically by the parameters. $Pr$ has no substantial effect on $f$, while $Nu$ is considerably increased, when a strong secondary current is present beforehand. On the contrary, $Ro$ causes a great increase in $f$, but $Nu$ is much less enhanced. The increase in them due to $Gr_2$ is gradual. However, it has an advantageous characteristic that it makes more contribution to the enhancement of heat transfer than flow friction. $K_1$ also possesses the same advantage, and raises more rapidly both $f$ and $Nu$.

Since the tube wall exercises a resistant force against the secondary flow, its rise and intensity are largely dependent on the geometrical shape of tube cross section. It is apparant that the circular cross section has a less resistance against the current so that the secondary flow occurs more readily, and its effects on $f$ and $Nu$ appear at much smaller values for a circular tube. The threshhold values of the non-dimensional force parameters at which their effects begin to be pronounced are $Ro \approx 2$, $Gr_2 \approx 100$ and $K_1 \approx 100$ for a circular tube, while they are $Ro \approx 10$, $Gr_2 \approx 1000$ and $K_1 \approx 100$ for a square tube. The rate of increase in $f$ and $Nu$ due to the force parameters is also higher for a circular tube for the same reason.

## ACKNOWLEDGEMENT

The author wishes to thank the University of Minnesota Computer Center for the grant extended to him of computation time on the CDC 6600 Computer.

## REFERENCES

1. S. N. Barua, Secondary flow in a rotating straight pipe, *Proc. R. Soc.* **227A**, 133 (1954).
2. W. D. Morris, Laminar convection in a heated vertical tube rotating about a parallel axis, *J. Fluid Mech.* **21**, 453 (1965).
3. J. F. Humphreys, W. D. Morris and H. Barrow, Convection heat transfer in the entry region of a tube which revolves about an axis parallel to itself, *Int. J. Heat Mass Transfer* **10**, 333 (1967).
4. Y. Mori and W. Nakayama, Forced convective heat transfer in a straight pipe rotating about a parallel axis (1st report, laminar region), *Int. J. Heat Mass Transfer* **10**, 1179 (1967).
5. W. R. Dean, Note on the motion of fluid in a curved pipe, *Phil. Mag.* **4** (20), 208 (1927).
6. W. R. Dean, The stream line motion of fluid in a curved pipe, *Phil. Mag.* **5** (30), 673 (1928).
7. M. Adler, Strömung in gekrümmten Rohren, *Z. Angew. Math. Mech.* **14**, 257 (1934).
8. S. N. Barau, On secondary flow in stationary curved tubes, *Q. J. Mech. Appl. Math.* **16**, 61 (1963).
9. Y. Mori and W. Nakayama, Study on forced convective heat transfer in curved pipes (1st report, laminar region), *Int. J. Heat Mass Transfer* **8**, 67 (1965).
10. Y. Mori and W. Nakayama, Study on forced convective heat transfer in curved pipes (2nd report, turbulent region), *Int. J. Heat Mass Transfer* **10**, 37 (1967).
11. H. Ito, Friction factors for turbulent flow in curved pipes, *J. Basic Engng* **81D**, 123 (1959).
12. R. A. Seban and E. F. McLaughlin, Heat transfer in tube coils with laminar and turbulent flow, *Int. J. Heat Mass Transfer* **6**, 387 (1963).
13. G. C. F. Rogers and Y. R. Mayhew, Heat transfer and pressure loss in helically coiled tubes with turbulent flow, *Int. J. Heat Mass Transfer* **7**, 1207 (1964).
14. H. Ludwieg, Die ausgebildete Kanalströmung in einem rotierenden System, *Ing.-Archiv* **19**, 77 (1959).
15. H. Miyazaki, Combined free and forced convective heat transfer and fluid flow in rotating curved tubes, MS Thesis, University of Minnesota (1970).
16. D. B. Spalding, A. K. Runchal and M. Wolfshtein, Solutions of the equations for the transport of vorticity, heat and mass for two-dimensional flows with and without recirculation, Imperial College, Mech. Eng. Depart., SF/TN/2 (1967).
17. L. A. Dorfman and U. B. Romanenko, Flow of viscous fluid in cylindrical vessel with rotating cover (in Russian), *AH CCCP, Mech. Fluid Gas* (5), 63 (1966).

## CONVECTION THERMIQUE MIXTE NATURELLE ET FORCÉE POUR UN FLUIDE DANS UN TUBE COURBE EN ROTATION

**Résumé**—On étudie la convection thermique mixte naturelle et forcée pour un fluide dans un tube courbe et à section circulaire en rotation avec les conditions d'un écoulement complètement établi et de flux thermique pariétal constant par unité de longueur de tube. Les caractéristiques du transfert thermique et du frottement pariétal sont déterminées par cinq paramètres sans dimension: le rapport des rayons $B$, le nombre de Prandtl $Pr$, un paramètre $R_0$ qui représente l'effet des forces de Coriolis, le nombre de Grashof $Gr_2$ et le nombre de Dean $K_1$. Les équations sont résolues par la méthode des différences finies et les résultats du calcul sont présentés pour les profils de vitesse longitudinale, les lignes de courant et les isothermes, les $Nu$ et $f$ locaux et moyens. Les effets de $B$ sont minimes. $Pr$ n'a pas d'effet sensible sur $f$ mais accroît notablement $Nu$ quand un fort courant secondaire est présent. L'accroissement des trois derniers paramètres relatifs à l'induction du courant secondaire intensifie à la fois $f$ et $Nu$. Le taux d'accroissement de $f$ et $Nu$ dû à ces paramètres est plus élevé pour un tube circulaire que pour un tube rectangulaire. Leurs effets commencement à être prononcés aux valeurs inférieures $Ro \approx 2$, $Gr_2 \approx 100$ et $K_1 \approx 100$ tandis que pour un tube carré $Ro \approx 10$, $Gr_2 \approx 1000$ et $K_1 \approx 100$.

## WÄRMEÜBERGANG UND STRÖMUNG IN EINEM ROTIERENDEN, GEKRÜMMTEN KREISROHR BEI KOMBINIERTER FREIER UND ERZWUNGENER KONVEKTION

**Zusammenfassung**—Die kombinierte freie und erzwungene konvektive Wärmeübertragung und die Strömungsausbildung in einem rotierenden Kreisrohr bei voll entwickelter Strömung mit der thermischen Randbedingung eines konstanten Wärmestroms pro Längeneinheit des Rohres wurden untersucht. Die Wärmeübertragung und der Reibungseinfluss der Strömung wurden durch fünf dimensionslose Parameter erfasst, das sind das Radiusverhältuis $B$, die Prandtl-Zahl $Pr$, der Parameter $R_0$, der den Einfluss der Corioliskraft berücksichtigt, die Grashof-Zahl $Gr_2$ und die Dean-Zahl $K_1$. Die beschreibenden Gleichungen wurden mit einem endlichen Differenzenverfahren gelöst und die Ergebnisse der Berechnung sind angegeben für die Axial-Geschwindigkeit und die Temperaturstörung, die Stromlinien und die Isothermen, die lokalen $f$ und $Nu$ und die mittleren $f$ und $Nu$.

Der Einfluss von $B$ ist minimal. $Pr$ hat grundsätzlich keinen Einfluss auf $f$, aber zunehmendes $Nu$ vergrössert $f$, wenn ein Sekundär-Strom vorhanden ist. Die Zunahme in den letzten drei Parametern der sekundär-induzierten Strömungskräfte vergrössert sowohl $f$ als auch $Nu$ grundsätzlich. Die Grösse der Zunahme in $f$ und $Nu$, abhängig von den Kraft-Parametern, ist für ein Kreisrohr höher als für ein Rechteck-Rohr. Ihr Einfluss beginnt merklich bei kleineren Parametern als $Ro \approx 2$, $Gr_2 \approx 100$ und $K_1 \approx 100$, während diese Grenzen für ein quadratisches Rohr bei $Ro \approx 10$, $Gr_2 \approx 1000$ und $K_1 \approx 100$ liegen.

## ТЕПЛООБМЕН И ТЕЧЕНИЕ ПРИ СОВМЕСТНОЙ СВОБОДНОЙ И ВЫНУЖДЕННОЙ КОНВЕКЦИИ ВО ВРАЩАЮЩЕЙСЯ ИСКРИВЛЕННОЙ ТРУБЕ КРУГЛОГО СЕЧЕНИЯ

**Аннотация**—Исследуется сложный теплообмен свободной и вынужденной конвекцией и течение жидкости во вращающейся искривленной круглой трубе для полностью развитого течения. Тепловой поток на единицу длины трубы предполагается постоянным. Определены характеристики теплообмена и сопротивления потоку с помощью пяти безразмерных параметров: отношения радиусов $B$, числа Прандтля $Pr$, параметра $R_0$, представляющего влияния кориолисовой силы, числа Грасгофа $Gr_2$ и числа Дина $K_1$. Основные уравнения решены методом конечных разностей. Представлены распределения аксиальной скорости и температуры, линий тока и изотерм локального $f$ и $Nu$, и средних $f$ и $Nu$. Показано, что влияние $B$ минимально. $Pr$ не оказывает существенного влияния на $f$, но значительно увеличивает $Nu$ при наличии сильного вторичного тока. Увеличение последних трех параметров, ответственных за силы, индуцирующие вторичные течения, значительно усиливает $f$ и $Nu$. Скорость возрастания $f$ и $Nu$ из-за этих параметров для круглой трубы больше, чем для труб прямоугольных. Их влияние начинает существенно сказываться при их значениях гораздо меньших, чем значения $Ro \approx 2$, $Gr_2 \approx 100$ и $K_1 \approx 100$, тогда как для квадратных труб $Ro \approx 10$, $Gr_2 \approx 1000$ и $K_1 \approx 100$.